

# Fuzzy Sliding Mode Control of Rigid-Flexible Multibody Systems With Bounded Inputs

**Pinhas Ben-Tzvi**

Department of Mechanical and Aerospace  
Engineering,  
School of Engineering and Applied Science,  
The George Washington University,  
801 22nd Street, NW,  
Washington, DC 20052

**Shengjian Bai**

**Qingkun Zhou**

**Xinsheng Huang**

College of Mechatronics Engineering and  
Automation,  
National University of Defense Technology,  
Changsha Hunan 410073,  
People's Republic of China

*This paper presents the dynamic modeling and fuzzy sliding mode control for rigid-flexible multibody systems. To investigate the dynamic stiffening of rigid-flexible systems, a first-order approximate model of a flexible spacecraft system is formulated by using Hamilton's principles and assumed mode method, taking into account the second-order term of the coupling deformation field. For highly flexible structural models, ideal surface sliding that produces pure rigid body motion may not be achievable. In this paper, the discontinuity in the sliding mode controller is smoothed inside a thin boundary layer using fuzzy logic technique to reduce the chattering phenomenon efficiently. Sliding mode control is insensitive to parameter variations and provides complete rejection of disturbances, but these advantages only hold in the sliding mode domain. However, when the actuators' amplitude is limited by their physical constraints, the sliding mode domain will be restricted to some local domain near zero on the switching surface. Control input saturation is also considered in the fuzzy sliding mode control approach. The new features and advantages of the proposed approach are the use of new dynamic equations for the motion of flexible spacecraft systems and the design of fuzzy sliding mode control by taking into account the control input saturation. The classical sliding mode control case is also developed for comparison. Numerical simulations are performed to validate the proposed methods and to demonstrate that rotational maneuvers and vibration suppression are accomplished in spite of the presence of model uncertainty and control saturation nonlinearity. [DOI: 10.1115/1.4004581]*

*Keywords:* dynamic stiffening, sliding mode control, fuzzy logic, flexible structures, vibrations, saturation

## 1 Introduction

Mechanical systems operating at high-speed can produce a phenomenon referred to as dynamic stiffening due to the coupling between rigid motion and elastic deflection [1], and traditional dynamic analysis techniques can hardly deal with this. Recent research activities indicate that the second-order term in the coupling deformation field has a “stiffening” effect on the system's frequencies [1–3]. In this paper, we take into account the second-order term of the coupling deformation field, and obtain the first-order approximate model (FOAM) of a flexible spacecraft model.

Modern space exploration is leading to ever more demanding performance criteria, such as high rotational speeds and large angular maneuverability, increased precision, and pointing accuracy. Several recent studies on linear and nonlinear control of flexible satellites have been performed [4–7].

Sliding mode control (SMC) is recognized as a powerful theoretical technique for robust control, even under variations in system parameters or the presence of external disturbances [8]. Several representative research works are available in the literature on SMC theory [9–16]. For different mission objectives, various control techniques have been developed and compared [13–16]. SMC for a three axis rotational maneuver of a highly flexible spacecraft model is proposed in Ref. [13], where the control structure takes the flexibility effect into consideration. A sliding mode attitude control algorithm with an exponential time-varying sliding surface is designed in Ref. [14], which guarantees the occurrence of the sliding mode at the beginning and eliminates the reaching phase of time-invariant SMC. Fuzzy control is used

in Ref. [15] to approximate the equivalent control of SMC via regulation rules in the presence of the satellite parameter uncertainties and external disturbances. Fuzzy rules are employed to smooth the sign function in Ref. [6]. In order to prevent the presence of input saturation from significantly degrading the system's performance, a saturation compensator is designed in Ref. [16] for the sliding mode attitude control system. Nevertheless, research work on the FOAM of flexible spacecrafts remains rare [7].

The robustness of SMC only holds in the sliding mode domain (SMD) on all switching surfaces, which is easily satisfied without input saturation. However, in reality, spacecraft actuators' amplitude is practically limited by physical constraints. Therefore, SMD is not the whole switching surface and will be restricted to some local domain near zero on the switching surface. The motion outside the SMD is so-called “bang-bang” motion, which lacks any robustness. Thus, the design of an SMC input that is constrained by saturation is studied in this paper. Also, by using fuzzy logic (FL) techniques, the discontinuity in the sliding mode controller is smoothed inside a time-varying boundary layer so as to reduce the chattering phenomenon efficiently.

## 2 Equations of Motion and Kinematics

Figure 1 depicts a model for slewing flexible spacecrafts with a rigid central hub and two elastic beams attached to it. The beams represent structural elements of a spacecraft such as an on-board antenna and solar arrays. Although the design approach of the present work can be applied to multiaxial maneuvers, only single-axis maneuvers are considered in this paper for simplicity. The spacecraft is controlled by a torque  $T$  on the rigid hub. When the spacecraft is maneuvered, the elastic members connected to the hub undergo structural deformation.

The coordinate axes  $XY$  and  $xy$  in Fig. 1 are defined as the inertial and reference frames, respectively.  $\bar{u}_P$  denotes the flexible

Contributed by the Dynamic Systems Division of ASME for publication in the JOURNAL OF DYNAMIC SYSTEMS, MEASUREMENT AND CONTROL. Manuscript received September 14, 2009; final manuscript received April 12, 2011; published online November 11, 2011. Assoc. Editor: Rama K. Yedavalli.

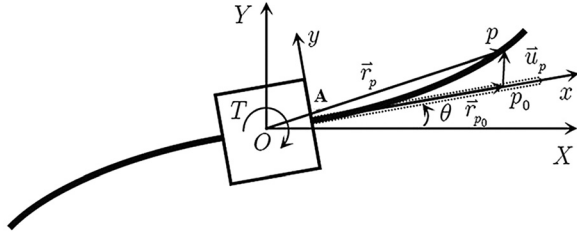


Fig. 1 Flexible spacecraft model

deformation vector at point  $P$  with respect to the  $xy$  frame, while  $\vec{r}_A$  is the radius vector of point  $A$  on the hub and  $\theta$  is a rigid body coordinate. After deformation, point  $P_0$  moves to point  $P$ .

The beam is characterized by a length  $L$ , with material properties  $E$  and  $\rho$  denoting the modulus of elasticity and the mass per unit volume of the beam, respectively, and cross-sectional proper-

ties  $A$  and  $I$  denoting the beam cross-sectional area and the area moment of inertia, respectively.

The deformation vector  $u_p$  can be represented by the following expression [3]:

$$u_p = (u_1 \quad u_2)^T = (w_1 + w_c \quad w_2)^T \quad (1)$$

where  $w_1$  represents the pure axial deformation of the centroidal axis and  $w_2$  denotes the transverse deformation along the  $y$ -axis of the reference frame  $xy$ . The second-order term  $w_c$  is defined as

$$w_c = -\frac{1}{2} \int_0^x \left( \frac{\partial w_2}{\partial x} \right)^2 dx \quad (2)$$

It should be noted that this term can have a significant impact on the beam's dynamic equations when it undergoes large rigid-body motion.

By applying Hamilton's principles, the first-order model (FOM) of the flexible spacecraft can be written as

$$\left. \begin{aligned} & \int_0^L \left\{ \rho A w_1 - 2\rho A \dot{\theta} \dot{w}_2 - \rho A \ddot{\theta} w_2 - \rho A \dot{\theta}^2 (r_A + w_1 + x) - EA w_1'' \right\} dx = 0 \\ & \int_0^L \left\{ \rho A \ddot{w}_2 + 2\rho A \dot{\theta} \dot{w}_1 + \rho A \ddot{\theta} (r_A + w_1 + x) - \rho A \dot{\theta}^2 w_2 - EI w_2'''' + \rho A \frac{\partial}{\partial x} \left[ w_2' \int_x^L B(\xi, t) d\xi \right] \right\} dx = 0 \\ & 2 \int_0^L \left\{ \rho A \left\{ \ddot{\theta} [(r_A + x)^2 + w_1^2 + w_2^2 + 2(r_A + x)(w_1 + w_c)] + (r_A + w_1 + x) \ddot{w}_2 \right. \right. \\ & \quad \left. \left. - w_2 \ddot{w}_1 + 2\dot{\theta} [(r_A + x)(\dot{w}_1 + \dot{w}_c) + w_1 \dot{w}_1 + w_2 \dot{w}_2] \right\} dx + J_h \ddot{\theta} = T \right\} \end{aligned} \right\} \quad (3)$$

where

$$B(x, t) = -\dot{\theta}^2 (r_A + x + w_1 + w_c) - 2\dot{\theta} \dot{w}_2 + \ddot{w}_1 + \ddot{w}_c - \ddot{\theta} w_2 \quad (4)$$

The boundary conditions are

$$\left. \begin{aligned} w_1(0, t) = 0, \quad w_2(0, t) = 0, \quad w_1'(0, t) = 0 \\ EI w_2''(L, t) = 0, \quad EA w_1'(L, t) = 0, \quad EI w_2'''(L, t) = 0 \end{aligned} \right\} \quad (5)$$

Then, by using Assumed Mode Method (AMM) and deleting the high order terms of the generalized coordinates, the FOAM of the flexible spacecraft model can be derived as

$$\begin{aligned} & \begin{bmatrix} M_{\theta\theta} & M_{\theta q_1} & M_{\theta q_2} \\ M_{q_1\theta} & M_{q_1 q_1} & \mathbf{0} \\ M_{q_2\theta} & \mathbf{0} & M_{q_2 q_2} \end{bmatrix} \begin{bmatrix} \ddot{\theta} \\ \ddot{q}_1 \\ \ddot{q}_2 \end{bmatrix} + 2\dot{\theta} \begin{bmatrix} 0 & \mathbf{0} & \mathbf{0} \\ 0 & \mathbf{0} & \mathbf{G}_{q_1 q_2} \\ 0 & \mathbf{G}_{q_2 q_1} & \mathbf{0} \end{bmatrix} \begin{bmatrix} \dot{\theta} \\ \dot{q}_1 \\ \dot{q}_2 \end{bmatrix} \\ & + \begin{bmatrix} 0 & \mathbf{0} & \mathbf{0} \\ 0 & \mathbf{K}_{q_1 q_1} & \mathbf{0} \\ 0 & \mathbf{0} & \mathbf{K}_{q_2 q_2} \end{bmatrix} \begin{bmatrix} \theta \\ q_1 \\ q_2 \end{bmatrix} = \begin{bmatrix} Q_\theta \\ Q_{q_1} \\ Q_{q_2} \end{bmatrix} + \begin{bmatrix} \tau \\ \mathbf{0} \\ \mathbf{0} \end{bmatrix} \quad (6) \end{aligned}$$

where  $M_{\theta\theta} \in R^1$  is the rotary inertia of the system and  $M_{q_1 q_1} \in R^{n \times n}$  and  $M_{q_2 q_2} \in R^{n \times n}$  are the beam's generalized elastic mass matrices.  $M_{\theta q_1} \in R^{1 \times n}$ ,  $M_{\theta q_2} \in R^{1 \times n}$ ,  $M_{q_1 \theta} \in R^{n \times 1}$ , and  $M_{q_2 \theta} \in R^{n \times 1}$  represent the nonlinear inertia coupling between the motion of the reference frame and the elastic deformations.  $\mathbf{K}_{q_1 q_1} \in R^{n \times n}$  and  $\mathbf{K}_{q_2 q_2} \in R^{n \times n}$  are the generalized elastic stiffness matrices that are shown to be affected by both the motion of the reference frame and the elastic deformations.  $Q_\theta$ ,  $Q_{q_1}$ , and  $Q_{q_2}$  represent inertia forces and  $\tau = T$  is the external rotational torque.  $q_1(t)$  and  $q_2(t)$  represent the vectors of the generalized coordinates for axial and transverse displacements, respectively.  $\mathbf{G}_{q_1 q_2}$  and

$\mathbf{G}_{q_2 q_1}$  are constant matrices resulting from gyroscopic effects. It should be noted that in transitioning from Eq. (3) to Eq. (6),  $T$ ,  $w_1$ , and  $w_2$  were replaced by  $\tau$ ,  $q_1$ ,  $q_2$ ,  $\phi_1$ , and  $\phi_2$ , such that  $\tau = T$ ,  $w_1 = \phi_1 q_1$ , and  $w_2 = \phi_2 q_2$  with  $\phi_1$  and  $\phi_2$  defined after Eq. (22). The matrices in Eq. (6) are given as follows:

$$M_{\theta\theta} = J_h + J_b + q_1^T M_1 q_1 + q_2^T M_2 q_2 + 2V_1 q_1 - \underline{q_2^T D q_2} \quad (7)$$

$$M_{q_1 \theta} = M_{\theta q_1}^T = -R q_2 \quad (8)$$

$$M_{\theta q_2} = M_{q_2 \theta}^T = V_2 + q_1^T R \quad (9)$$

$$M_{q_i q_i} = M_i \quad i = 1, 2 \quad (10)$$

$$\mathbf{G}_{q_1 q_2} = -\mathbf{G}_{q_2 q_1}^T = -R \quad (11)$$

$$\mathbf{K}_{q_1 q_1} = \mathbf{K}_1 - \dot{\theta}^2 M_1 \quad (12)$$

$$\mathbf{K}_{q_2 q_2} = \mathbf{K}_2 - \dot{\theta}^2 M_2 + \underline{\dot{\theta}^2 D} \quad (13)$$

$$Q_\theta = -2\dot{\theta} \left[ (q_1^T M_1 \dot{q}_1 + q_2^T M_2 \dot{q}_2) + V_1 \dot{q}_1 - \underline{q_2^T D \dot{q}_2} \right] \quad (14)$$

$$Q_{q_1} = \dot{\theta}^2 V_1^T \quad (15)$$

where  $J_b$  is the rotational inertia of the flexible appendages about the hub's center and  $J_h$  is the rotational inertia of the central rigid body.

The nonlinear coupling between the rigid-body motion and the elastic deformation in Eq. (6) can be easily seen. The underlined terms in Eqs. (7), (13), and (14) result from the coupling deformation field. The newly established Eqs. (23)–(32) are called the FOAM, and the equations without the underlined terms are called traditional linear approximate model (TLAM).

The constant coefficients and matrices in Eqs.(7)–(15) are

$$J_b = \int_0^L \rho A (r_A + x)^2 dx \quad (16)$$

$$\mathbf{K}_1 = \int_0^L EA \left( \frac{\partial \phi_1(x)}{\partial x} \right)^T \frac{\partial \phi_1(x)}{\partial x} dx \quad (17)$$

$$\mathbf{K}_2 = \int_0^L EI \left( \frac{\partial^2 \phi_2(x)}{\partial x^2} \right)^T \frac{\partial^2 \phi_2(x)}{\partial x^2} dx \quad (18)$$

$$\mathbf{M}_i = \int_0^L \rho A \phi_i^T \phi_i dx, \quad i = 1, 2 \quad (19)$$

$$\mathbf{V}_i = \int_0^L \rho A (r_A + x) \phi_i dx, \quad i = 1, 2 \quad (20)$$

$$\mathbf{D} = \int_0^L \rho A (r_A + x) S(x) dx \quad (21)$$

$$\mathbf{R} = \int_0^L \rho A \phi_1^T \phi_2 dx \quad (22)$$

where matrices  $\mathbf{K}_1 \in R^{n \times n}$  and  $\mathbf{K}_2 \in R^{n \times n}$  are the conventional stiffness matrices, and  $\mathbf{M}_i \in R^{n \times n}$  ( $i = 1, 2$ ) are generalized elastic mass matrices. Matrix  $\mathbf{D}$  results from the second-order term of the coupling deformation field given by Eq. (2), and matrix  $\mathbf{R}$  results from gyroscopic effects.  $\phi_1$  and  $\phi_2$  represent the vectors of the admissible functions of axial displacement and transverse displacement, respectively.  $S(x)$  is derived from  $w_c$  and is represented by

$$S(x) = \int_0^x \frac{\partial \phi_2^T(\xi)}{\partial \xi} \frac{\partial \phi_2(\xi)}{\partial \xi} d\xi \quad (23)$$

It is important to note that matrix  $\mathbf{D}$  is non-negative definite since  $S(x)$  itself is non-negative definite as well.

A simplified first-order approximate model (SFOAM) of the flexible spacecraft can be derived from FOAM by deleting the elements related to  $Q_\theta$ ,  $q_1$ , and  $\dot{q}_1$ . Therefore, Eq. (6) reduces to

$$\begin{bmatrix} M_{\theta\theta} & M_{\theta q_2} \\ M_{q_2\theta} & M_{q_2 q_2} \end{bmatrix} \begin{bmatrix} \ddot{\theta} \\ \ddot{q}_2 \end{bmatrix} + \begin{bmatrix} 0 & \mathbf{0} \\ \mathbf{0} & \mathbf{K}_{q_2 q_2} \end{bmatrix} \begin{bmatrix} \theta \\ q_2 \end{bmatrix} = \begin{bmatrix} \tau \\ \mathbf{0} \end{bmatrix} \quad (24)$$

where  $M_{\theta\theta}$ ,  $M_{\theta q_2}$  ( $M_{q_2\theta}$ ),  $M_{q_2 q_2}$ , and  $\mathbf{K}_{q_2 q_2}$  can be obtained by deleting the elements related to  $q_1$  and  $\dot{q}_1$  in Eqs. (7), (9), (10), and (13), respectively. The elements  $Q_\theta$ ,  $q_1$ , and  $\dot{q}_1$  could be ignored while obtaining SFOAM because the inertia forces  $Q_\theta$  are much smaller than the control input  $\tau$ , while  $q_1$  and  $\dot{q}_1$  are much smaller compared to the other state variables  $q_2$ ,  $\dot{q}_2$ ,  $\theta$ , and  $\dot{\theta}$ . Recall that  $q_1$  represents the axial displacement of the flexible appendage, and as such it is very small compared to  $q_2$  and  $\theta$  ( $q_2$  represents the transverse displacement of the flexible appendage and  $\theta$  represents the angular displacement of the rigid central body). The small element  $Q_{q_2}$  is also deleted for simplicity.

It is noted that SFOAM will be used for the controller design.

### 3 Fuzzy Sliding Mode Controller Design

In order to maneuver the rotation angle from  $\theta_0$  to  $\theta_d$ , we design a control law  $u(t)$  which satisfies the following constraints:

$$\begin{aligned} \lim_{t \rightarrow \infty} q_i(t) &= \lim_{t \rightarrow \infty} \dot{q}_i(t) = 0 \quad (i = 1, 2, \dots, n) \\ \lim_{t \rightarrow \infty} \theta(t) &= \theta_d, \quad \lim_{t \rightarrow \infty} \dot{\theta}(t) = 0 \end{aligned} \quad (25)$$

**3.1 Design of Sliding Mode Control.** As the next step, the design of Fuzzy Sliding Mode Control (FSMC) will be investigated by using the Reaching Law Method [17] and FL. SMC has evolved into a major design tool for controlling nonlinear systems, but its inherent chattering is an obstacle in practice. In this section,

the Reaching Law Method and Fuzzy Time-varying Boundary Layer Thickness are adopted to achieve a trade-off between tracking precision and robustness to modeling inaccuracies.

The following nonlinear system in a companion form is considered

$$\text{Plant : } x^{(n)}(t) = f(\mathbf{x}, t) + b(\mathbf{x}, t)u(t) + d(t) \quad (26)$$

$$\text{Model : } x^{(n)}(t) = \hat{f}(\mathbf{x}, t) + \hat{b}(\mathbf{x}, t)u(t) \quad (27)$$

where  $\mathbf{x} = [x, \dot{x}, \dots, x^{(n-1)}]^T$  is the state vector,  $u(t)$  is the scalar control input, and  $d(t)$  is the external disturbance. Assume that the nonlinear function  $f(\mathbf{x}, t)$  and  $d(t)$  are not exactly known, then

$$f(\mathbf{x}, t) = \hat{f}(\mathbf{x}, t) + \Delta f(\mathbf{x}, t) \quad (28)$$

and

$$\begin{aligned} |\Delta f(\mathbf{x}, t)| &< F(\mathbf{x}, t) \\ |d(t)| &< D(t) \end{aligned} \quad (29)$$

where  $\hat{f}(\mathbf{x}, t)$ ,  $\Delta f(\mathbf{x}, t)$ , and  $F(\mathbf{x}, t)$  represent the known model of the system, model uncertainties, and upper bound for uncertainties, respectively.  $D(t)$  is the upper bound of  $d(t)$ . Furthermore, we assume that  $b(\mathbf{x}, t)$  is not exactly known, then

$$0 < b_{\min} < b(\mathbf{x}, t) < b_{\max}, \quad b(\mathbf{x}, t) \neq 0 \quad \forall t \quad (30)$$

and

$$\hat{b}(\mathbf{x}, t) = (b_{\min} b_{\max})^{1/2} \quad (31)$$

Let  $\mathbf{e} = \mathbf{x} - \mathbf{x}_d = [x - x_d, \dot{x} - \dot{x}_d, \dots, x^{(n-1)} - x_d^{(n-1)}]$  be the tracking error and let us define a time-varying sliding surface  $s(\mathbf{e})$  as

$$s(\mathbf{e}) = \sum_{i=1}^n c_i e_i, \quad c_n = 1, \quad \text{and} \quad c_i > 0 \quad (32)$$

where  $e_i = x^{(i-1)} - x_d^{(i-1)}$ , for  $i = 1, 2, \dots, n$ , and the characteristic polynomial of Eq. (32) is Hurwitz. The design parameters  $c_i$  determine the response speed in the sliding mode and the steady state response of the system, which will be discussed in Sec. 4.

Three approaches for specifying the reaching condition have been proposed [18] as follows:

- (a) The direct switching function approach, with the condition

$$s\dot{s} < 0 \quad (33)$$

- (b) The Lyapunov function approach, with the condition

$$s\dot{s} < -\eta|s| \quad (34)$$

where  $\eta$  is a positive constant.

- (c) The reaching law approach, with the condition

$$\dot{s} = -\eta \text{sgn}(s) - ks \quad (35)$$

where  $\eta$  and  $k$  are positive constants. The reaching condition provided in Eq. (33) is global, but does not guarantee a finite reaching time. On the other hand, the reaching laws described in Eqs. (34) and (35) not only have global characteristics but also guarantee a finite reaching time.

A thin boundary layer in the neighborhood of the switching surface is used here to smooth out the control discontinuity as shown in Fig. 2, thus eliminating chattering

$$B(\mathbf{x}, t) = \{x, |s(\mathbf{x}, t)| \leq \phi(t)\} \quad \phi(t) > 0 \quad (36)$$

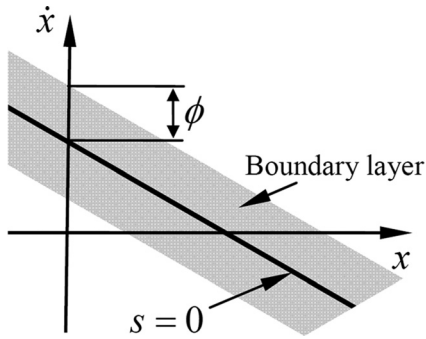


Fig. 2 The boundary layer

When all trajectories that start inside  $\phi_0(t=0)$  remain inside  $\phi(t)$  for all  $t \geq 0$ , we interpolate  $u(t)$  inside  $\phi(t)$  as illustrated in Fig. 3.

In the case of variable boundary layers, the control input  $u(t)$  in Eq. (26) is made to satisfy the following reaching condition [19]:

$$s\dot{s} \leq -(\eta - \dot{\phi})|s| \quad (37)$$

where  $\eta$  is a strictly positive constant and  $\phi(t)$  is the boundary layer thickness.

Comparison of Eqs. (37) and (34) shows that because of the added term  $\dot{\phi}|s|$ , the boundary layer attraction condition is more stringent during boundary layer contraction ( $\dot{\phi} < 0$ ) and less stringent during boundary layer expansion ( $\dot{\phi} > 0$ ) [19].

By differentiating Eq. (32) and rearranging it using Eq. (26), we obtain

$$\dot{s} = \sum_{i=1}^{n-1} c_i e_{i+1} - x_d^{(n)} + f(x, t) + b(x, t)u(t) + d(t) \quad (38)$$

Also, by combining the reaching condition given by Eq. (37) and the reaching law from Eq. (35), we obtain a novel reaching law with time-varying boundary layer as follows:

$$\dot{s} = -(\eta - \dot{\phi})\text{sat}(s/\phi) - ks \quad (39)$$

where

$$\text{sat}(s/\phi) = \begin{cases} s/\phi, & \text{for } |s/\phi| \leq 1 \\ \text{sgn}(s/\phi), & \text{for } |s/\phi| > 1 \end{cases} \quad (40)$$

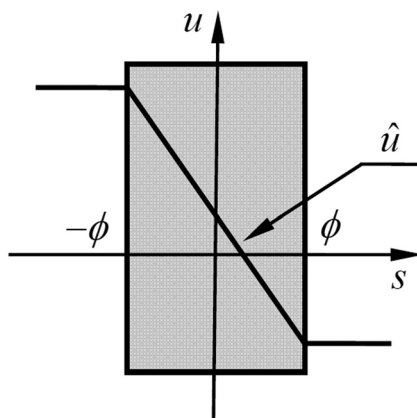


Fig. 3 Control interpolation in the boundary layer

The advantage of the proposed novel reaching law described by Eq. (13) is to reduce chattering by tuning the parameters  $\eta$  and  $k$  [8]. The boundary layer here is used to achieve a trade-off between tracking precision and robustness.

The control input can be derived from Eqs. (26), (27), and (39) as follows:

$$u(t) = \hat{u}(t) - \hat{b}^{-1}(x, t)k(x, t)\text{sat}(s/\phi) \quad (41)$$

$$\hat{u}(t) = \hat{b}^{-1}(x, t) \left[ x_d^{(n)} - \sum_{i=1}^{n-1} c_i e_{i+1} - \hat{f}(x, t) - k \sum_{i=1}^n c_i e_i \right] \quad (42)$$

where

$$k(x, t) = b^{-1}(x, t)\hat{b}(x, t) \left[ F(x, t) + D(t) + \eta - \dot{\phi}(t) \right] + |b^{-1}(x, t)\hat{b}(x, t) - 1| |\hat{u}(t)| \quad (43)$$

Note that

$$b^{-1}(x, t)\hat{b}(x, t) \leq \beta$$

where  $\beta = (b_{\max}/b_{\min})^{1/2}$ . Equation (43) can be rewritten as

$$k(x, t) \leq \beta \left[ F(x, t) + D(x, t) + \eta - \dot{\phi}(t) \right] + (\beta + 1)|\hat{u}(t)| \quad (44)$$

It can be seen that the control parameter  $k$  has been increased in order to account for the uncertainty on the control gain  $b$ , parameter uncertainty, and disturbance.

**3.2 Design of Fuzzy Boundary Layer.** The introduction of the boundary layer around the switching surfaces reduces chattering at the cost of increasing the tracking error. The variable boundary layer is a popular solution to this problem. In this section, FL is used to improve the performance of the sliding mode controller. The fuzzy boundary layer leads to a strategy that involves the adjustment of the boundary thickness automatically. This fuzzy system adopts the sliding surfaces  $s$  and  $\dot{s}$  as the inputs and the boundary layer thickness  $\phi$  as the output.

The Multiple Input-Single Output rule base is presented in Table 1, where ZR, SS, MM, and LL are used as abbreviations for zero, small, medium and large, respectively.

The input/output fuzzy membership functions are shown in Fig. 4.

The results interpreted by the fuzzy rule are shown in Fig. 5, which shape the thickness of the boundary layer.

**3.3 Design of Linear Switching Line With Bounded Inputs.** In this section, the sliding mode domain and the reaching domain of SMC are investigated with bounds on the control action. We aim at achieving robustness in the maximized sliding mode domain on the switching surfaces.

First, we consider the design of SMC for the following single-input Linear Time Invariant (LTI) system with bounded input

$$\dot{x} = Ax + Bu \quad |u| \leq K, \quad K > 0 \quad (45)$$

Table 1 Fuzzy rules for  $s$ ,  $\dot{s}$ , and  $\phi$

		s			
		ZR	SS	MM	LL
phi	ZR	ZR	ZR	SS	SS
	SS	ZR	SS	SS	MM
	MM	SS	SS	MM	LL
	LL	SS	MM	LL	LL

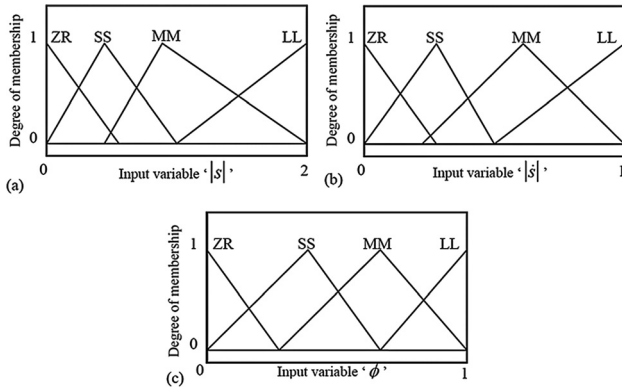


Fig. 4 Membership functions for  $s$ ,  $\dot{s}$ , and  $\phi$

The state vector  $x$  is  $n$ -dimensional,  $A$  and  $B$  are constant matrices of appropriate dimensions. A linear switching surface is selected as

$$s := Sx = 0 \quad (46)$$

where  $S$  is  $n$ -dimensional vector,  $SB = 1$ , and  $(n - 1)$  poles of the equivalent system are stable

$$\dot{x} = (I - BS)x \quad (47)$$

where  $I$  is a unity matrix.

The choice of the following control law:

$$u = -SAx - Ksgn(s), \quad K > 0 \quad (48)$$

guarantees that the trajectory of the solution of Eq. (45) globally reaches on to the switching surface given by Eq. (46) within a finite time and is constrained on it. In this case, the closed-loop system is represented by the following reaching law [17]:

$$\dot{s} = -Ksgn(s) \quad (49)$$

which satisfies the following reaching condition:

$$s\dot{s} < 0 \quad (50)$$

On one hand, when the input of the system described by Eq. (45) is constrained by severe saturation, the control law (48) cannot be applied directly. On the other hand, control inputs for real systems are always bound to saturate, but studies on SMC from this perspective are rare [7,8].

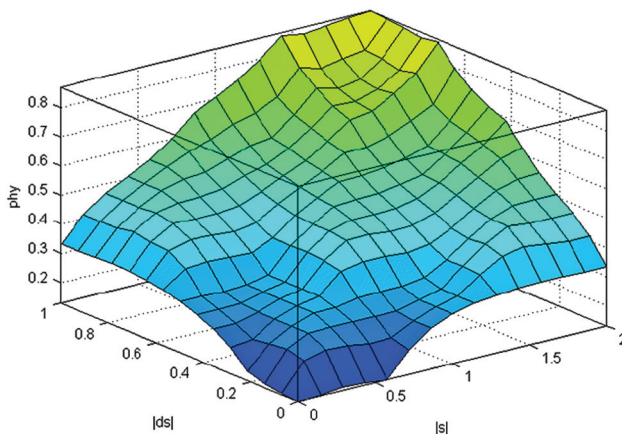


Fig. 5 3D plot of  $s$ ,  $\dot{s}$ , and  $\phi$

We first investigate the design of SMC for LTI systems whose inputs are constrained. That is, for a single-input LTI system as described by Eq. (45), where the input is constrained in advance based on the following condition:

$$|u| \leq K, \quad K > 0 \quad (51)$$

The following bounded control law

$$u = -Ksgn(s) \quad (52)$$

is considered. The question therefore is how to select the switching surface  $s(x) = 0$  in order to maximize the sliding mode domain.

As preliminary consideration, the following definitions are given.

**Definition 1 (Ref. [3]).** If, for any  $x_0$  on the switching surface  $s = 0$ , we have  $x(t)$  on  $s = 0$  for all  $t > t_0$ , then  $x(t)$  is a sliding motion or sliding mode of the system.

Based on the above definition, the following three definitions are derived:

**Definition 2.** A domain  $D$  on the switching surface  $s = 0$  is a sliding mode domain (SMD) if every point on it undergoes the sliding motion.

**Definition 3.** A domain  $M$  in the state-space is a reaching domain (RD) if the reaching condition given by Eq. (50) is satisfied in the domain.

**Definition 4.** A domain  $M$  in the state-space is an inescapable reaching domain (URD) if the motion starting from any initial state within  $M$  reaches on to SMD within a finite time  $T$ .

Concerning the above definitions, the following statements hold true:

- With the input constraint described in Eq. (51), the SMD is not necessarily the whole switching surface, and it is often restricted to some local domain near zero in the state-space.
- The SMD is a subspace of the switching surface, in which the reaching condition is satisfied.
- A point inside the URD does not necessarily satisfy reaching conditions, that is, RD is a subspace of URD.

The closed-loop system can be viewed as Lur'e-type system. Namely, a memoryless nonlinear feedback as provided by Eq. (52) to the forward LTI system belongs to the sector  $[0, \infty)$ . If the transfer function of the linear subsystem is so-called positive real, then it possesses important properties which may lead to the generation of a Lyapunov function for the whole system.

The following two lemmas describe a positive linear system and its stability:

**Lemma 1 (Ref. [18]).** A minimum realization of the following LTI system

$$G(s) = C(sI - A)^{-1}B + D \quad (53)$$

is given by

$$\begin{aligned} \dot{x} &= Ax + Bu \\ y &= Cx + Du \end{aligned} \quad (54)$$

The system described by Eq. (54) is strictly passive if  $G(s)$  is strictly positive real.

**Lemma 2(Ref. [18]).** The following strictly passive system is considered:

$$\begin{aligned} \dot{x} &= f(x, u) \\ y &= h(x, u) \end{aligned} \quad (55)$$

The origin of  $\dot{x} = f(x, 0)$  is globally asymptotically stable if a storage function of the system given by Eq. (55) is radial unbounded.

Based on the **Lemmas** and **Definitions** presented above, global stabilization of the LTI system (45) by the bounded control given by Eq. (52) is considered. The following theorem is valid.

**Theorem.** For the system given by Eq. (54), if  $A$  is Hurwitz and  $(A, B)$  is controllable, then by choosing the stable switching surface

$$s(x) := Sx = 0 \quad (56)$$

where  $SB = 1$  and  $(S, A)$  is observable, the SMD becomes

$$D := \{x | Sx = 0, -K < SAx < K\} \quad (57)$$

and the URD is the whole state-space.

**Proof.** First, concerning definition 2 and the linear switching surface described in Eq. (56), we have

$$\begin{cases} \dot{s} = S(Ax + BK) > 0 & s < 0 \\ \dot{s} = S(Ax - BK) < 0 & s > 0 \end{cases} \quad (58)$$

That is,

$$-K < SAx < K$$

Therefore, the SMD is as given by Eq. (57).

Second, concerning the fact that the LTI system is a minimum realization of the strict positive transfer function given by Eq. (53) [19]; according to Lemma 1, the LTI system is strictly passive. A radial unbounded Lyapunov function can be chosen as a storage function by using KYP lemma as provided in Ref. [18]. Therefore, according to Lemma 2, it is guaranteed that the closed loop system is globally exponentially stable. So if a ball  $N$  near zero is considered such that

$$N(x, \gamma) := \{x \in R^n | \|x\| \leq \gamma\} \quad (59)$$

where

$$0 < \gamma \leq \frac{K}{\|SA\|}, \quad (60)$$

the initial state from any point of the state-space reaches inside the ball within a finite time. That is, the initial state from any point of the state-space approaches the SMD given by Eq. (57) within a finite time.

The control approach given by Eq. (52) guarantees that the trajectory of the solution starting from any initial state of the system described in Eq. (45) reaches on to the sliding mode domain (57) on the switching surface within a finite time and approaches zero thereafter.

In order to illustrate, a rigid spacecraft undergoing single-axis maneuver will be investigated for simplicity. Its equation of motion is given by

$$J\ddot{\theta} = T \quad (61)$$

where  $J$  is the rotational inertia of the rigid spacecraft and  $T$  is a constant rotational torque, which is constrained by

$$|T| \leq U, \quad U > 0 \quad (62)$$

Without loss of generality, it is assumed that the flexible spacecraft maneuvers start at an initial angle  $\theta_0$  and end at final angle  $\theta_d = 0$ . A linear switching line is defined as

$$s = \dot{\theta} + c\theta, \quad c > 0 \quad (63)$$

where  $c$  is the slope of the linear switching line, which cannot be chosen arbitrarily with bounded inputs.

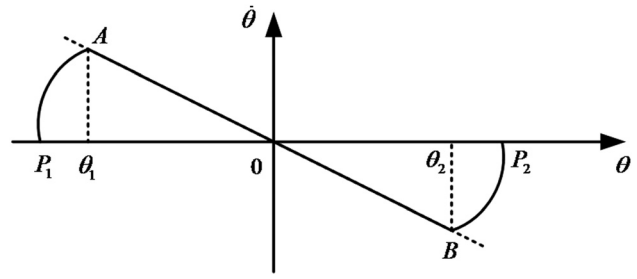


Fig. 6 sliding mode domain on linear switching line

As shown in Fig. 6,  $P_1$  and  $P_2$  are the initial points  $(\theta_0, 0)$  in the phase plane. With the restriction on the input as described in Eq. (62), based on the above theorem, the following expression can be derived showing that the SMD on the switching line is restrained to the local domain  $AB$  near zero

$$D_{\text{SMD}} = \left\{ (\theta, \dot{\theta}) \mid \dot{\theta} + c\theta = 0, \quad |\theta| < \left| \frac{\sqrt{U^2 - 2UJc^2\theta_0} - U}{Jc^2} \right| \right\} \quad (64)$$

The SMD is maximized when the optimized coefficient  $c$  is chosen as

$$c^* = \sqrt{\frac{3U}{2J|\theta_0|}} \quad (65)$$

## 4 Simulations and Results

In this section, simulation results for the dynamics of flexible spacecrafts are obtained using MATHEMATICA, VISUAL C and MATLAB/SIMULINK software. A slewing maneuver of a spacecraft is used to demonstrate the applicability of the FSMC in Secs. 2 and 3. A fourth-order Runge-Kutta program with adaptive step-size is used to numerically solve the differential equations. The physical parameters of the flexible hub-beam system are shown in Table 2.

### 4.1 Free Vibrations of the Flexible Spacecraft System.

Consider the flexible spacecraft model, as shown in Fig. 1. The free vibration mode of the FOAM and TLAM will be investigated. The angular velocity of the hub starts from zero and follows the following profile:

$$\dot{\theta} = \begin{cases} \frac{w_0}{T}t - \frac{w_0}{2\pi} \sin\left(\frac{2\pi}{T}t\right), & 0 \leq t \leq T \\ w_0, & t > T \end{cases} \quad (66)$$

where  $T = 10$  sec, and  $w_0 = 6$  rad/s.

Figure 7 shows the tip deflection of the beam using the two models. It can be seen from the figure that there is a significant deviation between the tip deflections when using TLAM (dashed line) compared to FOAM (solid line).

As can be seen from Fig. 7, the amplitude of the resulting tip deflection using the TLAM approach becomes much larger than that of the FOAM at  $t = 3.5$  s. Furthermore, the resulting tip deflection using the TLAM approach has exceeded the initial

Table 2 Physical parameters

Property	Symbol	Value
Beam length	$L$	12 m
Mass per unit volume	$\rho$	$2.8 \times 10^3 \text{ kg/m}^3$
Cross-Section	$A$	$7.5 \times 10^{-5} \text{ m}^2$
Young's modulus	$E$	$7.0 \times 10^{10} \text{ N/m}^2$
Beam area moment of inertia	$I$	$7.2 \times 10^{-9} \text{ m}^4$
Hub moment of inertia	$J_h$	$500 \text{ kg} \cdot \text{m}^2$
Hub radius	$r$	0.5 m

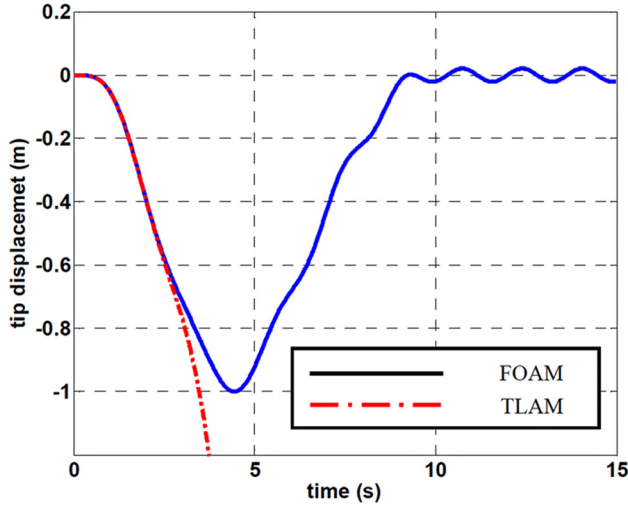


Fig. 7 Tip displacement response of the flexible appendages using FOAM and TLAM approaches

assumption of small deformations. Because the second-order term in the deformation field is not included, the elastic stiffness matrix may be negative definite and the system becomes unstable. From the above result, it is shown that the second-order term in the deformation field can have a significant effect on the dynamic behavior of flexible multibody systems at high-speeds. In fact, it can be calculated that the critical angular velocity is 2.2 rad/s [20]. If the angular velocity of the rotating central body exceeds the critical angular velocity, the deformation of flexible appendages will be infinite. It can be concluded that TLAM is invalid in describing the deformation of flexible multibody systems in high-speed cases.

**4.2 Fuzzy Sliding Mode Control of the Flexible Spacecraft Model.** By rearranging Eq. (24), the following expression is derived:

$$(M_{00} - M_{0q_2} M_{q_2 q_2}^{-1} M_{q_2 0}) \ddot{\theta} = \tau + M_{0q_2} M_{q_2 q_2}^{-1} K_{q_2 q_2} q_2 \quad (67)$$

The control input can be obtained the same way Eq. (41) was derived, namely

$$\tau = \hat{u}(t) - \hat{b}^{-1}(x, t) k(x, t) \text{sat}(s/\phi) \quad (68)$$

where

$$\hat{u}(t) = -(M_{00} - M_{0q_2} M_{q_2 q_2}^{-1} M_{q_2 0}) c \dot{\theta} - M_{0q_2} M_{q_2 q_2}^{-1} K_{q_2 q_2} q_2 \quad (69)$$

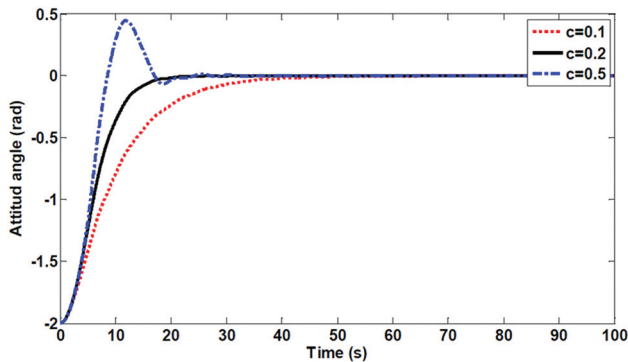


Fig. 8 Attitude angle

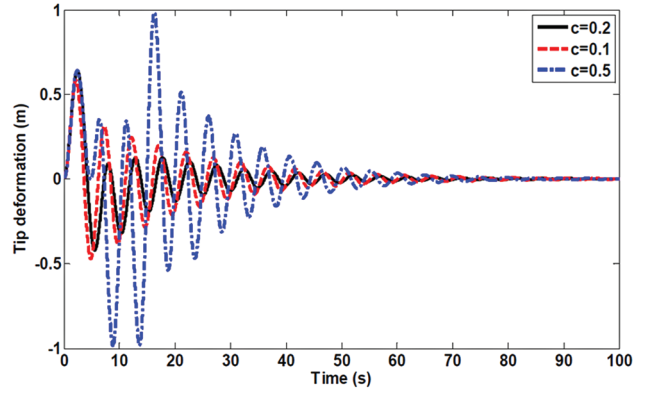


Fig. 9 Tip deformation of flexible appendages

$$k(x, t) = \beta [F(x, t) + D(t) + \eta - \dot{\phi}(t)] + (\beta + 1)|\dot{u}(t)| \quad (70)$$

and

$$f(x, t) = \frac{M_{0q_2} M_{q_2 q_2}^{-1} K_{q_2 q_2} q_2}{M_{00} - M_{0q_2} M_{q_2 q_2}^{-1} M_{q_2 0}} \quad (71)$$

The proposed controller derived from SFOAM is used for “rest-rest” attitude maneuvering of FOAM. Our aim is to maneuver the attitude of the spacecraft from  $\theta_0 = 2 \text{ rad}$  to  $\theta_d = 0$  and suppress the flexible vibration simultaneously. The control parameters are selected as  $F(x, t) = 0.5|\dot{f}(x, t)|$ ,  $\hat{b} = 1$ ,  $\beta = 2$ ,  $D(t) = 0$ ,  $\eta = 0$ ,  $c^* = 0.2$ , and  $K = 50 \text{ Nm}$ .

Although we are dealing with an infinite-dimensional system, it is impossible to use infinite number of modes in the simulation. To make the simulation more meaningful, the following two measures are taken: (i) a relative large number of flexible modes is chosen in the FOAM, which is used for the simulation; (ii) feedback signals associated with flexibility are assumed to be of the first mode since the lower frequency component is dominant [20]. Thus, the assumed modes  $n$  of FOAM and SFOAM are chosen as 5 and 1, respectively.

Figure 8 shows the attitude angle of the flexible spacecraft. According to that figure, it can be concluded that attitude angle control was accomplished in the closed-loop system. When  $c$  is chosen as 0.5, the time response of the attitude angle has an overshoot, whereas when  $c$  is chosen as 0.1, a longer settling time is depicted.

In the control of the flexible appendage, we are mainly interested in the motion of the tip, as described in Fig. 9. It can be observed that larger or smaller  $c$  values exhibit large tip deformations. Thus,

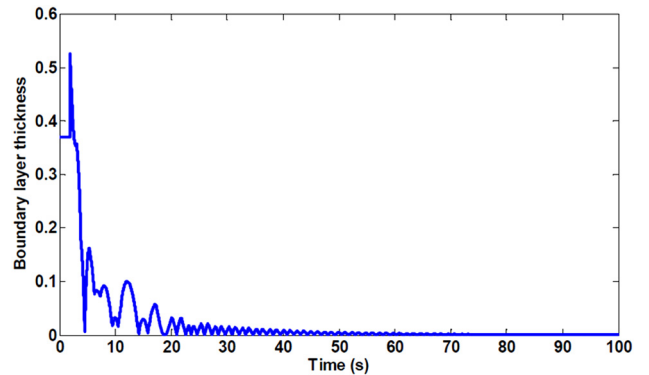


Fig. 10 Time-varying boundary layers

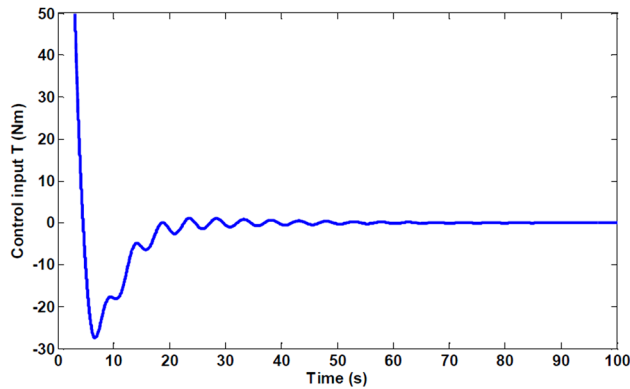


Fig. 11 Control input

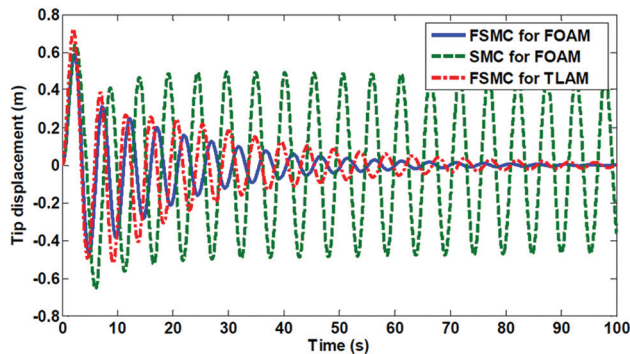


Fig. 12 Tip deformation

the parameter  $c$  discussed in Sec. 3.3 not only meets precision criteria of attitude angle but also exhibits small tip deformation.

Figure 10 shows that the thickness of the boundary layer  $\phi$  decays with time when using fuzzy logic. It can also be seen from the bounded control input shown in Fig. 11 that the use of boundary layer eliminates the chattering and generates a continuous control scheme.

Simulations were performed for both functions  $\text{sgn}(\cdot)$  and  $\text{sat}(\cdot)$  with boundary layers. It is clear from the tip displacement of the flexible appendage shown in Fig. 12 that (a) the residual vibration amplitude for the controller with  $\text{sat}(\cdot)$  is much smaller than that of  $\text{sgn}(\cdot)$ ; (b) the tip displacement is reduced using FSMC based on TLAM; however, it is still larger than that based on FOAM; (c) the tip displacement of FOAM is smaller than that of TLAM using FSMC, which can be attributed to dynamic stiffening effects. Namely, as can be seen in Eq. (13), the underlined term increases the stiffness matrix of FOAM when the flexible spacecraft undergoes attitude maneuvers, which acts as a “stiffening” effect. Moreover, the angular velocity of the flexible spacecraft does not exceed 0.4 rad/s, which is less than the critical angular velocity. It can be concluded that FSMC based on FOAM has better effect on reducing the tip displacement.

## 5 Conclusions

This paper presented the development of the first-order approximate model, traditional linear approximate model, and simplified first-order approximate model for rigid-flexible multibody systems. Free vibrations of the first-order approximate model and traditional linear approximate model were investigated to illustrate the validity of the first-order approximate model when experiencing high rotational speeds. The proposed control law was examined using fuzzy logic and sliding mode control theories with input saturation. Numerical simulations were provided to show the effectiveness of the proposed controller for rotational maneuvers and vibration suppression in spite of the presence of model uncertainty and control saturation nonlinearity.

## References

- [1] Kane, T. R., Ryan, R. R., and Banerjee, A. K., 1987, “Dynamics of a Cantilever Beam Attached to a Moving Base,” *J. Guid. Control Dyn.*, **10**(2), pp. 139–150.
- [2] Bai, S., Ben-Tzvi, P., Zhou, Q., and Huang, X., 2008, “Dynamic Modeling of a Rotating Beam Having a Tip Mass,” ROSE 2008—IEEE International Workshop on Robotic and Sensors Environments Proceedings, Ottawa, Canada, pp. 52–57.
- [3] Liu, J., and Hong, J., 2004, “Geometric Stiffening Effect on Rigid-Flexible Coupling Dynamics of an Elastic Beam,” *J. Sound Vib.*, **278**(4), pp. 1147–1162.
- [4] Hyland, D. C., Junkins, J. L., and Longman, R. W., 1993, “Active Control Technology for Large Space Structures,” *J. Guid. Control Dyn.*, **16**(5), pp. 801–821.
- [5] Hu, Q., 2008, “Sliding Mode Maneuvering Control and Active Vibration Damping of Three-Axis Stabilized Flexible Spacecraft With Actuator Dynamics,” *Nonlinear Dyn.*, **52**(3), pp. 227–248.
- [6] Guan, P., Liu, X. J., and Liu, J. Z., 2005, “Adaptive Fuzzy Sliding Mode Control for Flexible Satellite,” *Eng. Appl. Artif. Intell.*, **18**(4), pp. 451–459.
- [7] Cai, G. P., and Hong, J. Z., 2005, “Active Position Control of a Flexible Manipulator,” *Mech. Sci. Technol.*, **24**(1), pp. 70–74.
- [8] Hung, J. Y., Gao, W. B., and Hung, J. C., 1993, “Variable Structure Control. A Survey,” *IEEE Trans. Ind. Electron.*, **40**(1), pp. 2–22.
- [9] Diong, B. M., 2004, “Sliding-Mode Control Design for a Class of Systems With Non-Matching Nonlinearities and Disturbances,” *Int. J. Syst. Sci.*, **35**(8), pp. 445–455.
- [10] Hall, C. E., and Shtessel, Y. B., 2006, “Sliding Mode Disturbance Observer-Based Control for a Reusable Launch Vehicle,” *J. Guid. Control Dyn.*, **29**(6), pp. 1315–1328.
- [11] Bokovic, J. D., Li, S.-M., and Mehra, R. K., 2001, “Robust Adaptive Variable Structure Control of Spacecraft Under Control Input Saturation,” *J. Guid. Control Dyn.*, **24**(1), pp. 14–22.
- [12] Xu, Y. J., 2005, “Sliding Mode Control and Optimization for Six DOF Satellite Formation Flying Considering Saturation,” *J. Astronaut. Sci.*, **53**(4), pp. 433–443, <http://direct.bl.uk/bld/PlaceOrder.do?UIN=192832157&ETOC=RN&from=searchengine>.
- [13] Bang, H., Ha, C.-K., and Kim, J. H., 2005, “Flexible Spacecraft Attitude Maneuver by Application of Sliding Mode Control,” *Acta Astronaut.*, **57**, pp. 841–850.
- [14] Cong, B. L., Liu, X. D., and Chen, Z., 2010, “Exponential Time-Varying Sliding Mode Control for Large Angle Attitude Eigenaxis Maneuver of Rigid Spacecraft,” *Chin. J. Aeronaut.*, **23**, pp. 447–453.
- [15] Guan, P., Liu, X. J., and Liu, J. Z., 2005, “Adaptive Fuzzy Sliding Mode Control for Flexible Satellite,” *Artif. Intell.*, **18**, pp. 451–459.
- [16] Hu, Q. L., 2008, “Input Shaping and Variable Structure Control for Simultaneous Precision Positioning and Vibration Reduction of Flexible Spacecraft With Saturation Compensation,” *J. Sound Vib.*, **318**, pp. 18–35.
- [17] Gao, W. B., 1990, *Fundamentals of Variable Structure Control Theory*, Press of Science and Technology in China (in Chinese), Beijing, pp. 52–89.
- [18] Gao, W., and Hung, J. C., 1993, “Variable Structure Control of Nonlinear Systems. A New Approach,” *IEEE Trans. Ind. Electron.*, **40**(1), pp. 45–55.
- [19] Slotine, J. J. E., and Li, W., 1991, *Applied Nonlinear Control*, Prentice-Hall.
- [20] Bai, S., Ben-Tzvi, P., Zhou, Q., and Huang, X., 2009, “A Study on Dynamic Stiffening of a Rotating Beam with a Tip Mass,” *Sens. Transducers J.*, **5** (Special Issue), pp. 53–68.